Inverse scattering for high-resolution interferometric microscopy

Tyler S. Ralston, Daniel L. Marks, Stephen A. Boppart, and P. Scott Carney

Beckman Institute for Advanced Science and Technology, Department of Electrical and Computer Engineering, University of Illinois at Urbana-Champaign, 405 North Mathews Avenue, Urbana, Illinois 61801

We extend the applicability of inverse scattering for optical coherence tomography (OCT) to the case of high numerical aperture focusing optics. We include the effects of tight focusing so that the approach is applicable to any interferometric microscopy method. The applicability to modalities, such as OCT and optical coherence microscopy, enables computed reconstruction of three-dimensional volumes from *en face* temporal ranging data. Simulations show that the computed structure outside of the focal plane exhibits spatially invariant resolution on par with the resolution achieved at the focal plane. © 2006 Optical Society of America

OCIS codes: 110.4500, 100.3010, 100.3190, 290.3200, 100.6950.

High-resolution optical microscopy and tomography are of critical importance in modern biology and medicine, both in research and clinical applications. One particularly high-profile example is optical coherence tomography[1] (OCT). OCT is a ranging technique that relies on optical scattering to form micrometer-scale cross-sectional images[2] and has a wide range of medical applications.[3–5] A spatially invariant instrument response is critical to the diagnostic utility of OCT. Inverse scattering and computed imaging provide a means to obtain uniform resolution and quantitatively meaningful images in high-resolution OCT.[6] Moreover, the methods developed here are applicable to a wide range of optical modalities where the field is measured coherently in a two-dimensional (2D) manner across a finite spectral band.

It is conventionally assumed that in OCT the probing beam is both well collimated and well confined in directions transverse to the beam axis. The acquired signal then may be understood to represent a simple, 1D echogram of the object structure along the beam path. The time of flight of the returned signal is assumed to be proportional to the distance to the feature, and the amplitude of the returned signal is proportional to the strength of the scatterer or contrast with the background. Thus one may naively plot OCT data from a series of adjacent beam paths and obtain data that resemble a 3D rendering of the sample. In this way, the information content in OCT has been only minimally exploited, as little attention has been paid to the physics of the scattering and inverse scattering problems connecting data and object structure. Some attempts have been made to address the inverse scattering problem,[7] but, even there, the 1D model of field propagation was retained.

High-resolution OCT using short-coherence-length light sources has achieved axial resolutions of less than $1~\mu\mathrm{m}$.[8] The resolution of OCT in directions transverse to the beam axis is set by the numerical aperture (NA) of the optical system. To obtain high-resolution images, a high-NA optical system must be employed, but such a system is not commensurate with the assumption that the beam is well collimated. As a result, high-NA OCT systems produce high-fidelity images only in the focal plane. Images from data away from the focal plane have been considered unrecoverable, and therefore the nontomographic modality that results is called optical coherence microscopy[9] (OCM). The focal plane in OCM may be scanned axially to acquire a 3D image, but the data acquisition time then scales with an extra multiplicative factor of the number of focal planes.

In previous work,[6] a mathematical description of the forward problem connecting the object structure to the data measured in OCT was presented. It was shown that the object structure could be obtained as a function of the data by solution of the inverse scattering problem (ISP) in 3D and that the resultant images exhibited a spatially invariant resolution and, moreover, provided quantitatively meaningful data. In that work, the paraxial approximation was used. For higher-NA systems such an approach is not appropriate. Here we solve the ISP analytically without resorting to the paraxial approximation. The results are applicable to high-resolution microscopy and are demonstrated by numerical simulation.

OCT data are obtained by probing the sample with a beam and measuring the return or backscattered signal. There are many variations on the basic measurement scheme, and whether a time-domain method or a spectral-domain method is used, it is generally possible to obtain a complex analytic signal through interferometric means. A spectral-domain OCM[10] setup is shown in Fig. 1. Such a setup provides better phase stability and signal-to-noise ratio than the time-domain counterpart.[11,12] The necessary
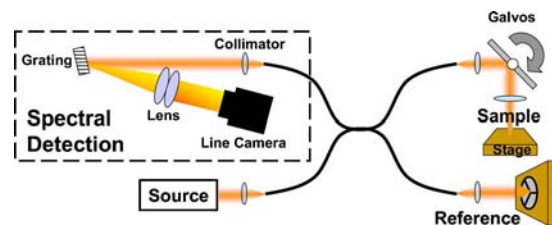

Fig. 1.   (Color online) System diagram for spectral-domain optical coherence microscopy. The system is composed of a broadband source, a fiber-based interferometer, and a spectral detector. Note that data are collected at the camera as the optical Fourier transform.

data may be acquired with the use of a low-coherence source or by use of a scanned-frequency source.

The beam orientation is assumed fixed while the axis is translated over the sample in directions orthogonal to the beam axis. Subsequent axial scans are displayed on adjacent lines. Suppose the collimated beam emerges from an optical fiber and then propagates through a lens to form a focused beam incident on the sample. With the axis of the fiber passing through the point $\mathbf{r}_0$ in the $z=0$ plane and with the waist plane of the focused field at $z=z_0$, the incident field may be described by the power spectrum $A^2(k)$ and a normalized mode g such that $U_i(\mathbf{r},\mathbf{r}_0,k)=A(k)g(\mathbf{r}-\mathbf{r}_0)$. The mode may be written in a plane wave decomposition

$$g(\mathbf{r}-\mathbf{r}_0,k) = \frac{1}{(2\pi)^2} \int \mathrm{d}^2q \, \exp[i\mathbf{q}(\mathbf{r}-\mathbf{r}_0)]$$
$$\times \exp[ik_z(\mathbf{q})(z-z_0)]\tilde{g}_0(\mathbf{q},k), \quad (1)$$

where $\tilde{g}_0$ is the 2D Fourier transform of g in the $z=z_0$ plane and the dispersion relation is given by $k_z(\mathbf{q})=\sqrt{k^2-q^2}$. The beam waist is assumed to depend on the wave number as $W_0(k)=\alpha/k$, where $\alpha=\pi/\mathrm{NA}$ and NA is the numerical aperture of the output lens. Thus $\tilde{g}_0(\mathbf{q},k)=\exp(-q^2W_0^2/2)=\exp[-q^2\alpha^2/(2k^2)]$. The scattered field, within the first Born approximation, is given by $U_s(\mathbf{r},\mathbf{r}_0,k)=\int\mathrm{d}^3r'G(\mathbf{r}',\mathbf{r},k)\times U_i(\mathbf{r}',\mathbf{r}_0,k)\eta(\mathbf{r}')$. Making use of the expressions above for the incident field,

$$U_s(\mathbf{r},\mathbf{r}_0,k) = A(k)\int \mathrm{d}^3r' G(\mathbf{r}',\mathbf{r},k)g(\mathbf{r}'-\mathbf{r}_0,k)\eta(\mathbf{r}'). \quad (2)$$

The signal coupled back into the fiber, as was shown in Ref. 6, is given by the projection of the backscattered field on to the fiber mode g at the exit plane of the fiber. Thus $S(\mathbf{r}_0,k)=\int_{z=0}\mathrm{d}^2rU_s(\mathbf{r},\mathbf{r}_0,k)g(\mathbf{r}-\mathbf{r}_0,k)$, which becomes

$$S(\mathbf{r}_0,k) = A(k)\int_{z=0} \mathrm{d}^2r \int \mathrm{d}^3r' G(\mathbf{r}',\mathbf{r},k)$$
$$\times g(\mathbf{r}'-\mathbf{r}_0,k)g(\mathbf{r}-\mathbf{r}_0,k)\eta(\mathbf{r}'). \quad (3)$$

The Green function for free-space propagation is given by the angular spectrum

$$G(\mathbf{r}',\mathbf{r},k) = \frac{i}{2\pi} \int \mathrm{d}^2q \, \exp[i\mathbf{q}(\mathbf{r}-\mathbf{r}')]$$
$$\times \frac{\exp[-ik_z(\mathbf{q})(z-z')]}{k_z(\mathbf{q})}, \quad (4)$$

where it is assumed that the scatterers are all located such that $z<z'$. Making use of this expression and Eq. (3), it may be seen that the 2D Fourier transform of S with respect to $\mathbf{r}_0$ is given by the expression

$$\tilde{S}(\mathbf{Q},k) = i2\pi A(k)\int \mathrm{d}^2q \int \mathrm{d}z' \frac{1}{k_z(\mathbf{q})} \exp[ik_z(\mathbf{q})(z'-z_0)]$$
$$\times \exp[ik_z(\mathbf{q}-\mathbf{Q})(z'-z_0)]$$
$$\times \exp\left(\frac{-\alpha^2q^2}{2k^2}\right)\exp\left(\frac{-\alpha^2|\mathbf{q}-\mathbf{Q}|^2}{2k^2}\right)\tilde{\eta}(\mathbf{Q},z'). \quad (5)$$

This equation may be solved for η by expensive numerical methods. An analytic result may be obtained by considering the form of the integral

$$\tilde{S}(\mathbf{Q},k) = i2\pi A(k)\int \mathrm{d}^2q \int \mathrm{d}z' \frac{1}{k_z(\mathbf{q})} \exp[ik_z(\mathbf{q})(z'-z_0)]$$
$$\times \exp[ik_z(\mathbf{q}-\mathbf{Q})(z'-z_0)]$$
$$\times \exp\left[\frac{-\alpha^2Q^2}{4k^2}\right]\exp\left[\frac{-\alpha^2|\mathbf{q}-\mathbf{Q}/2|^2}{k^2}\right]\tilde{\eta}(\mathbf{Q},z'). \quad (6)$$

For large values of α this integral may be evaluated asymptotically. The integrand, modulo the Gaussian, may be expanded in a Taylor series around the point $\mathbf{q}=\mathbf{Q}/2$

$$\frac{\exp\{i[k_z(\mathbf{q})+k_z(\mathbf{q}-\mathbf{Q})](z'-z_0)\}}{k_z(\mathbf{q})}$$
$$= \frac{\exp[2ik_z(\mathbf{Q}/2)(z'-z_0)]}{k_z(\mathbf{Q}/2)} + (\mathbf{q}-\mathbf{Q}/2)$$
$$\cdot \nabla_\mathbf{q}\frac{\exp\{i[k_z(\mathbf{q})+k_z(\mathbf{q}-\mathbf{Q})](z'-z_0)\}}{k_z(\mathbf{q})}\Bigg|_{\mathbf{q}=\mathbf{Q}/2} + \cdots, \quad (7)$$

where $\nabla_\mathbf{q}$ is the gradient with respect to $\mathbf{q}$. Replacing this part of the integrand, the leading term is given by an integral over the constant term in the Taylor expansion:

$$\tilde{S}(\mathbf{Q},k) = i2\pi A(k)\exp\left(\frac{-\alpha^2Q^2}{4k^2}\right)$$
$$\times \int \mathrm{d}z' \frac{\exp[2ik_z(\mathbf{Q}/2)(z'-z_0)]}{k_z(\mathbf{Q}/2)}$$
$$\times \int \mathrm{d}^2q \, \exp\left(\frac{-\alpha^2|\mathbf{q}-\mathbf{Q}/2|^2}{k^2}\right)\tilde{\eta}(\mathbf{Q},z'). \quad (8)$$

The Gaussian integral may be carried out, and the remaining integral is seen to be a Fourier transform with respect to z',

$$\tilde{S}(\mathbf{Q},k) = \frac{k^2}{\alpha^2}i2\pi^2A(k)\frac{\exp[-2ik_z(\mathbf{Q}/2)z_0]}{k_z(\mathbf{Q}/2)}$$
$$\times \exp\left(\frac{-\alpha^2Q^2}{4k^2}\right)\tilde{\eta}[\mathbf{Q},-2k_z(\mathbf{Q}/2)], \quad (9)$$

where $\widetilde{\widetilde{\eta}}$ is the 3D Fourier transform of η. The next term in the expansion yields a contribution proportional to α^{-4}. In the limit where NA$\rightarrow$1, it may be seen that $\alpha \rightarrow \pi$, so that we expect the leading term approximation to be sufficient even in the case of high NA. It might be noted that this expansion is distinct from the paraxial approximation [essentially a small $|\mathbf{q}|$ expansion of $k_z(\mathbf{q})$], which fails as NA$\rightarrow$1.

To find an appropriate regularization scheme, we write $\widetilde{S}(\mathbf{Q},k) = \int \mathrm{d}\beta H(\mathbf{Q},k,\beta)\widetilde{\widetilde{\eta}}(\mathbf{Q},\beta)$, where

$$H(\mathbf{Q},k,\beta) = \frac{k^2}{\alpha^2}i2\pi^2 A(k)\frac{\exp[-2ik_z(\mathbf{Q}/2)z_0]}{k_z(\mathbf{Q}/2)}$$

$$\times \exp\left(\frac{-\alpha^2 Q^2}{4k^2}\right)\delta[\beta + 2k_z(\mathbf{Q}/2)]$$

$$\equiv f(\mathbf{Q},k,\beta)\delta[\beta + 2k_z(\mathbf{Q}/2)]. \quad (10)$$

Then the kernel of the normal operator is given by the expression

$$H^*H(\mathbf{Q},\beta,\beta') \equiv |f(\mathbf{Q},1/2\sqrt{\beta^2 + Q^2},\beta)|^2$$

$$\times \frac{\beta}{2\sqrt{\beta^2 + Q^2}}\delta(\beta - \beta'), \quad (11)$$

so that the kernel of the Tikhonov regularized pseudo-inverse with a regularization constant N is given by the expression

$$H^+(\mathbf{Q},k;\beta) = \frac{f^*(\mathbf{Q},k,\beta)\delta(k - 1/2\sqrt{\beta^2 + \mathbf{Q}^2})}{|f(\mathbf{Q},k,\beta)|^2 + 2Nk/k_z(\mathbf{Q}/2)}. \quad (12)$$

The object structure is then given by

$$\widetilde{\widetilde{\eta}}^+(\mathbf{Q},\beta) = \left[\frac{f^*(\mathbf{Q},k,\beta)\widetilde{S}(\mathbf{Q},k)}{|f(\mathbf{Q},k,\beta)|^2 + 2Nk/k_z(\mathbf{Q}/2)}\right]_{k=\frac{1}{2}\sqrt{\beta^2 + \mathbf{Q}^2}}. \quad (13)$$

The object structure in the coordinate domain is obtained by applying the 3D inverse Fourier transform.

The results above are verified in a simulation. An OCM scan of an object consisting of point scatterers, randomly placed inside and outside of the scanning boundary, is simulated. The simulated object volume is 50 wavelengths in depth, and 20×45 wavelengths in the transverse directions. The illumination source has a Gaussian spectrum with a 40% fractional FWHM bandwidth (corresponding, for example, to 320 nm of bandwidth centered at 800 nm, with 1 μm axial resolution). The simulated NA of the imaging objective is 1. Gaussian noise is added to the simulated volume to attain an signal-to-noise ratio of 35 dB before reconstruction. The structure of the object is reconstructed from the data.

Figure 2(a) shows a 3D rendering of the simulated OCM volume. The projected volume is displayed in Fig. 2(c). After solving for the pseudo-inverse by using Eq. (13), it may be seen that the algorithm produces a spatially invariant resolution except for edge effects, Figs. 2(b) and 2(d). Our nonparaxial method properly rephases the scattered signal to produce
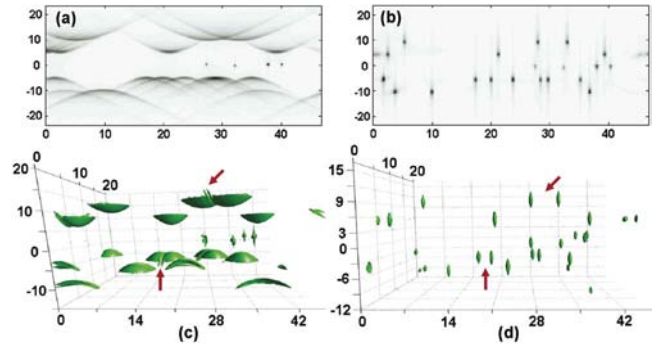

Fig. 2. (Color online) Simulated volume of point scatterers imaged with OCM to demonstrate spatially invariant resolution. Projection of (a) unprocessed and (b) processed data on a 2D plane, and full 3D rendering of (c) unprocessed and (d) processed volume of point scatterers. All axes are labeled in units of wavelength. Arrows in (c) indicate wavefront interference, which is resolved in (d).

spatially invariant resolution in a quantitatively meaningful reconstruction. This new capability has the potential to significantly enhance the utility and reliability for the family of interferometric microscopies as medical diagnostic and research tools. Future work will address attenuation of the signal away from the focus and polarization effects.

References

1. D. Huang, E. A. Swanson, C. P. Lin, W. G. Stinson, W. Chang, R. Hee, T. Flotte, K. Gregory, C. A. Puliafito, and J. G. Fujimoto, Science **254**, 1178 (1991).
2. B. E. Bouma and J. G. Tearny, *The Handbook of Optical Coherence Tomography* (Marcel Dekker, 2001).
3. C. Puliafito, M. Hee, C. Lin, E. Reichel, J. Schuman, J. S. Duker, J. A. Izatt, E. A. Swanson, and J. G. Fujimoto, Ophthalmology **102**, 217 (1995).
4. J. Schmitt, A. Knuttel, M. Yadlowsky, and M. Eckhaus, Phys. Med. Biol. **39**, 1705 (1994).
5. S. A. Boppart, B. E. Bouma, C. Pitris, J. F. Southern, M. E. Brezinski, and J. G. Fujimoto, Nat. Med. **4**, 861 (1998).
6. T. S. Ralston, D. L. Marks, P. S. Carney, and S. A. Boppart, J. Opt. Soc. Am. A **23**, 1027 (2006).
7. O. Bruno and J. Chaubell, Opt. Lett. **21**, 2049 (2003).
8. B. Povazay, K. Bizheva, A. Unterhuber, B. Hermann, H. Sattmann, A. F. Fercher, W. Drexler, A. Apolonski, W. J. Wadsworth, J. C. Knight, P. S. J. Russell, M. Vetterlein, and E. Scherzer, Opt. Lett. **27**, 1800 (2002).
9. J. A. Izatt, M. R. Hee, G. M. Owen, E. A. Swanson, and J. G. Fujimoto, Opt. Lett. **19**, 590 (1994).
10. C. Vinegoni, T. S. Ralston, W. Tan, W. Luo, D. L. Marks, and S. A. Boppart, Appl. Phys. Lett. **88**, 053901 (2006).
11. J. F. deBoer, B. Cense, B. H. Park, M. C. Pierce, G. J. Tearney, and B. E. Bouma, Opt. Lett. **28**, 2067 (2003).
12. M. Choma, M. Sarunic, C. Yang, and J. Izatt, Opt. Express **11**, 2183 (2003).